Extreme mass-ratio inspirals around a spinning horizonless compact object

Elisa Maggio[1], Maarten van de Meent[2], Paolo Pani[1]
[1] *Dipartimento di Fisica, "Sapienza" Università di Roma & Sezione INFN Roma1, Piazzale Aldo Moro 5, 00185, Roma, Italy and*
[2] *Max Planck Institute for Gravitational Physics (Albert Einstein Institute) Am Muühlenberg 1, 14476 Potsdam, Germany*

Extreme mass-ratio inspirals (EMRIs) detectable by the Laser Interferometer Space Antenna (LISA) are unique probes of the nature of supermassive compact objects. We compute the gravitational-wave signal emitted by a stellar-mass compact object in a circular equatorial orbit around a Kerr-like horizonless supermassive object defined by an effective radius and a reflectivity coefficient. The Teukolsky equations are solved consistently with suitable (frequency-dependent) boundary conditions, and the modified energy and angular-momentum fluxes are used to evolve the orbital parameters adiabatically. The gravitational fluxes have resonances corresponding to the low-frequency quasinormal modes of the central object, which can contribute significantly to the gravitational-wave phase. Overall, the absence of a classical event horizon in the central object can affect the gravitational-wave signal dramatically, with deviations even larger than those previously estimated by a model-independent analysis of the tidal heating. We estimate that EMRIs could potentially place the most stringent constraint on the reflectivity of supermassive compact objects at the remarkable level of $\mathcal{O}(10^{-6})\%$ and would allow to constrain various models which are not ruled out by the ergoregion instability. In particular, an EMRI detection could allow to rule out (or provide evidence for) signatures of quantum black-hole horizons with Boltzmann reflectivity. Our results motivate performing rigorous parameter estimations to assess the detectability of these effects.

I. INTRODUCTION

The defining feature of a classical black hole (BH) is being a perfect absorber, since its event horizon is a one-way, null hypersurface. Thus, any evidence of some partial *reflectivity* near a dark compact object would indicate a departure from the classical BH picture, while an upper bound on the reflectivity could help quantify the "BH-ness" of a dark compact source [1].

Gravitational-wave (GW) astronomy naturally provides the ideal setting to constrain the reflectivity of compact sources. In fact, one might argue that imperfect GW absorption should be the rule rather than the exception, since event horizons are very special and all known forms of matter interacts very weakly with GWs, even in extreme conditions [2–4]. On the contrary, owing to their horizon, BHs are dissipative systems which behave like a Newtonian viscous fluid [5–8]. A spinning Kerr BH absorbs radiation of frequency $\omega > m\Omega_H$ (where m is the azimuthal number of the wave and Ω_H is the BH angular velocity) but amplifies radiation of smaller frequency, due to superradiance (see [9] for a review).

In the last few years several studies explored the possibility to constrain the reflectivity of compact GW sources (see Refs. [1, 10] for some reviews), mostly modelling the post-merger "echo" signal from exotic compact objects (ECOs) [11–21] or deriving projected bounds on the so-called "tidal heating", namely the backreaction on the orbital motion from the tides raised during the coalescence [22–24]. In a comparable-mass binary, tidal heating enters the GW phase at high post-Newtonian order [25], and is therefore hard to measure [26]. On the other hand, tidal heating in extreme mass-ratio inspirals (EMRIs) can produce thousands of radians of accumulated orbital phase [27–31] while in the sensitivity band of the future space-based Laser Interferometer Space Antenna (LISA) [32]. Recently, this effect was studied to develop a test that can place very stringent and model-independent constraints on the reflectivity of supermassive objects [31, 33], which adds to other unparalleled EMRI-based tests of fundamental physics, such as no-hair theorem tests based on measurements of the multipolar structure of the central object [31, 34–38], constraints on extra degrees of freedom arising in modified gravity [39–43], and null-hypothesis tests based on the absence of tidal Love numbers [44]. Altogether, these tests suggest that EMRIs will be unique probes of the nature of supermassive objects (for recent reviews on these and other tests, see Refs. [1, 45–47]).

The phenomenological approach of Ref. [31] was to study a standard BH EMRI dynamics and to parametrize a certain amount of reflectivity at the object surface in terms of a constant reflectivity coefficient $|\mathcal{R}|^2$, assuming that a fraction $(1-|\mathcal{R}|^2)$ of the radiation is absorbed. Clearly, the BH limit is recovered as $\mathcal{R}\to 0$, whereas $|\mathcal{R}|^2=1$ corresponds to a perfectly-reflective object. According to the analysis in [31], EMRIs could provide an unparalleled constraint at the level of $|\mathcal{R}|^2 \lesssim 10^{-4}$, much more stringent than current and future echo searches [1, 18–20].

The main goal of our paper is to improve the analysis of Ref. [31] by studying a consistent model of compact horizonless object, defined by a certain compactness and (possibly frequency-dependent) reflectivity coefficient, which in turn modify the boundary conditions for radiation at the surface. In our model, tidal heating and partial reflection are not imposed by hand, but rather arise automatically from the boundary conditions. The latter also generically affect the dynamics as well as the quasinormal modes (QNMs) of the central object [3, 4, 21, 48]. The QNM spectrum typically contains low-frequency modes arising from long-lived, quasibound states, which might be resonantly excited during the inspiral [49–52]. The role of these resonances in the EMRI dynamics was studied in Ref. [51] for a perfectly-reflecting, nonspinning, quasi-Schwarzschild horizonless object, for which an analytical treatment of the problem is possible (see also Ref. [52] for a more recent study). Our framework allows to extend the analysis of Ref. [51] to the case of generic (and possi-

bly frequency-dependent) reflectivity coefficient and generic spin. As we shall show, at variance with the case studied in Ref. [51], in more generic situations the presence of resonances can provide an important contribution to the EMRI dynamics. We shall also show that, by taking a consistent model into account, the already very stringent potential bounds derived by Ref. [31] can be further improved by some orders of magnitude. Finally, we show that EMRI detections have the potential to rule out (or provide observational hints of) models of quantum-gravity BH horizons featuring a (frequency-dependent) Boltzmann reflectivity [53].

The rest of this paper is organized as follows. In Sec. II we present our analytical and numerical framework, which relies on solving the EMRI dynamics around an ECO to leading order in an adiabatic expansion. We present our results in Sec. III and finally conclude in Sec. IV. Through this work, we use $G = c = 1$ units.

II. SETUP

A. A model for a Kerr-like horizonless object

We analyze a spinning compact horizonless object whose exterior spacetime is described by the Kerr metric [3, 13, 54]. The vacuum region outside a spinning object is not necessarily described by a Kerr geometry due to the absence of the Birkhoff's theorem beyond spherical symmetry. However, in the BH limit any deviation from the multipolar structure of a Kerr BH dies off sufficiently fast within General Relativity or if modified-gravity[1] effects are confined near the compact object [55]. Explicit examples of this "hair-conditioner theorem" are given in Refs. [56–61]. In this case, a spinning horizonless object with a compactness close to the BH one can be described by the Kerr metric in the exterior spacetime and the properties of the interior can be modelled in terms of a reflectivity coefficient.

In Boyer-Lindquist coordinates, the line element outside the compact object reads

$$\begin{aligned} ds^2 \quad &= -\left(1-\frac{2Mr}{\Sigma}\right)dt^2+\frac{\Sigma}{\Delta}dr^2-\frac{4Mr}{\Sigma}a\sin^2\theta d\phi dt \\ &+\Sigma d\theta^2+\left[(r^2+a^2)\sin^2\theta+\frac{2Mr}{\Sigma}a^2\sin^4\theta\right]d\phi^2\,, \end{aligned} \tag{1}$$

where $\Sigma = r^2 + a^2\cos^2\theta$ and $\Delta = r^2 + a^2 - 2Mr$, with M and $J \equiv aM$ the total mass and spin of the object, respectively. We shall consider a horizonless compact object whose radius is located at

$$r_0 = r_+(1+\epsilon)\,, \tag{2}$$

where $r_+ = M + \sqrt{M^2 - a^2}$ is the location of the would-be horizon. Let us notice that the parameter ϵ is related to the compactness of the object, namely $M/r_0 \approx M/r_+(1-\epsilon)$ when $\epsilon \ll 1$. Motivated by models of microscopic corrections at the horizon scale, we shall mostly focus on the case in which $\epsilon \ll 1$. For example, if $r_0 \sim r_+ + l_P$ (where l_P is the Planck length, as suggested by some quantum-gravity inspired models [62]), then $\epsilon \sim 10^{-44}$ for a compact object with $M \sim 10^6\, M_\odot$ and spin $a/M = 0.9$.

The properties of the interior are parametrized in terms of a complex and frequency-dependent reflectivity coefficient $\mathcal{R}$. The $\mathcal{R} = 0$ case describes a totally absorbing compact object (which reduces to the standard BH case when $\epsilon \to 0$), whereas the $|\mathcal{R}|^2 = 1$ case describes a perfectly reflecting compact object. Intermediate values of $\mathcal{R}$ describe partially absorbing compact objects due to viscosity or dissipation within the object [3, 4, 14, 19, 21, 53].

B. Linear perturbations from a point particle

Let us consider the case of a point-like source orbiting around a central object (either a Kerr BH or a Kerr-like ECO) in a circular equatorial orbit. In line with the previous discussion, we assume that in the exterior of the object General Relativity is valid, at least approximately (this does not prevent beyond-General-Relativity corrections in the object interior and at the horizon scale, which can be parametrized by the reflectivity coefficient). Therefore, gravitational perturbations in the exterior can be described as in the Kerr BH case. We analyze the gravitational perturbation in the Newman-Penrose formalism.[2] The Weyl scalar Ψ_4 can be expanded as

$$\Psi_4 = \hat{\rho}^4 \sum_{\ell,m} \int_{-\infty}^{\infty} d\omega R_{\ell m\omega}(r)\, {}_{-2}S_{\ell m\omega}(\theta) e^{i(m\phi-\omega t)}\,, \tag{3}$$

where $\hat{\rho} = (r - ia\cos\theta)^{-1}$ and the sum runs over $\ell \geq 2$ and $-\ell \leq m \leq \ell$. The radial wavefunction $R_{\ell m\omega}(r)$ and the spin-weighted spheroidal harmonics ${}_{-2}S_{\ell m\omega}(\theta)e^{im\phi}$ obey to the Teukolsky's master equations [65–67]

$$\Delta^2 \frac{d}{dr}\left(\frac{1}{\Delta}\frac{dR_{\ell m\omega}}{dr}\right) - V(r)R_{\ell m\omega} = \mathcal{T}_{\ell m\omega}\,, \tag{4}$$

$$\begin{aligned} &\left[\frac{1}{\sin\theta}\frac{d}{d\theta}\left(\sin\theta\frac{d}{d\theta}\right) + a^2\omega^2\cos^2\theta - \left(\frac{m-2\cos\theta}{\sin\theta}\right)^2 \right. \\ &\left. + 4a\omega\cos\theta - 4 + {}_{-2}A_{\ell m\omega}\right] {}_{-2}S_{\ell m\omega} = 0\,, \end{aligned} \tag{5}$$

where the effective potential reads

$$V(r) = -\frac{K^2 + 4i(r-M)K}{\Delta} + 8i\omega r + \lambda\,, \tag{6}$$

with $K = (r^2 + a^2)\omega - am$, and the separation constants λ and ${}_{-2}A_{\ell m\omega}$ are related by $\lambda \equiv {}_{-2}A_{\ell m} - 2am\omega + a^2\omega^2 - 2$.

[1] Furthermore, in gravity theories with higher curvature corrections to General Relativity, the metric of a supermassive object is generically expected to be Kerr [43].

[2] Very recently, using the Sasaki-Nakamura perturbations, a similar formalism was used to study a point particle plunging onto a spinning compact horizonless object in the context of developing accurate echo waveforms [63] (see also Ref. [64]).

The polar part of the spin-weighted spheroidal harmonics is normalized such that

$$\int_{-1}^{1} |{}_{-2}S_{\ell m\omega}(\cos\theta)|^2 \, d\cos\theta = 1 \,. \tag{7}$$

The source term $\mathcal{T}_{\ell m\omega}$ is constructed by projecting the stress-energy tensor $T^{\alpha\beta}$ of a point-like source with respect to the Newman-Penrose tetrad, where [68]

$$T^{\alpha\beta} = \mu \frac{u^\alpha u^\beta}{\Sigma \sin\theta u^t} \delta\left(r - r(t)\right) \delta\left(\theta - \theta(t)\right) \delta\left(\phi - \phi(t)\right) \,, \tag{8}$$

with μ being the mass of the small orbiting body, $u^\alpha = dz^\alpha/d\tau$, $z^\alpha = (t, r(t), \theta(t), \phi(t))$ is the geodesic trajectory, and τ is the particle proper time. We define the mass ratio of the system as $q = \mu/M$. In the case of circular equatorial orbits, $\theta(t) = \pi/2$ and, for co-rotating orbits, the orbital radius is related to the orbital angular frequency by

$$\Omega = \sqrt{M}/(a\sqrt{M} + r^{3/2}) \,. \tag{9}$$

Equation (4) can be solved through the standard Green's function method using the solutions of the homogeneous Teukolsky's equation.

1. BH case

Let us first review the standard BH case. Owing to the presence of a horizon, the two independent homogeneous solutions have the following asymptotic behavior

$$R^{\rm in}_{\ell m\omega} \sim \begin{cases} B^{\rm trans}_{\ell m\omega} \Delta^2 e^{-ikr_*} & \text{as } r_* \to -\infty \\ r^3 B^{\rm ref}_{\ell m\omega} e^{i\omega r_*} + r^{-1} B^{\rm inc}_{\ell m\omega} e^{-i\omega r_*} & \text{as } r_* \to +\infty \end{cases} , \tag{10}$$

$$R^{\rm up}_{\ell m\omega} \sim \begin{cases} C^{\rm up}_{\ell m\omega} e^{ikr_*} + \Delta^2 C^{\rm ref}_{\ell m\omega} e^{-ikr_*} & \text{as } r_* \to -\infty \\ r^3 C^{\rm trans}_{\ell m\omega} e^{i\omega r_*} & \text{as } r_* \to +\infty \end{cases} , \tag{11}$$

where $k = \omega - m\Omega_H$, $\Omega_H = a/(2Mr_+)$ is the angular velocity at the horizon of the Kerr BH, and the tortoise coordinate is defined such that $dr_*/dr = (r^2 + a^2)/\Delta$. The inhomogeneous solution of the Teukolsky's equation (4) is constructed as [68]

$$\begin{aligned} R_{\ell m\omega} = \frac{1}{W_{\ell m\omega}} \Bigg\{ & R^{\rm up}_{\ell m\omega}(r) \int_{r_+}^{r} dr' \frac{\mathcal{T}_{\ell m\omega}(r') R^{\rm in}_{\ell m\omega}(r')}{\Delta^2(r')} \\ & + R^{\rm in}_{\ell m\omega}(r) \int_{r}^{\infty} dr' \frac{\mathcal{T}_{\ell m\omega}(r') R^{\rm up}_{\ell m\omega}(r')}{\Delta^2(r')} \Bigg\} \,, \end{aligned} \tag{12}$$

where $W_{\ell m\omega}$ is the Wronskian given by

$$\begin{aligned} W_{\ell m\omega} &= \Delta^{-1} \left(R^{\rm in}_{\ell m\omega} \frac{dR^{\rm up}_{\ell m\omega}}{dr} - R^{\rm up}_{\ell m\omega} \frac{dR^{\rm in}_{\ell m\omega}}{dr} \right) \\ &= 2i\omega C^{\rm trans}_{\ell m\omega} B^{\rm inc}_{\ell m\omega} \,. \end{aligned} \tag{13}$$

The inhomogeneous solution in Eq. (12) has the following asymptotic behavior

$$R_{\ell m\omega} \sim \begin{cases} Z^H_{\ell m\omega} \Delta^2 e^{-ikr_*} & \text{as } r_* \to -\infty \\ Z^\infty_{\ell m\omega} r^3 e^{i\omega r_*} & \text{as } r_* \to +\infty \end{cases} , \tag{14}$$

where

$$Z^H_{\ell m\omega} = C^H_{\ell m\omega} \int_{r_+}^{\infty} dr' \frac{\mathcal{T}_{\ell m\omega}(r') R^{\rm up}_{\ell m\omega}(r')}{\Delta^2(r')} \,, \tag{15}$$

$$Z^\infty_{\ell m\omega} = C^\infty_{\ell m\omega} \int_{r_+}^{\infty} dr' \frac{\mathcal{T}_{\ell m\omega}(r') R^{\rm in}_{\ell m\omega}(r')}{\Delta^2(r')} \,, \tag{16}$$

and

$$C^H_{\ell m\omega} = \frac{B^{\rm trans}_{\ell m\omega}}{2i\omega C^{\rm trans}_{\ell m\omega} B^{\rm inc}_{\ell m\omega}} \,, \quad C^\infty_{\ell m\omega} = \frac{1}{2i\omega B^{\rm inc}_{\ell m\omega}} \,. \tag{17}$$

The amplitudes $Z^H_{\ell m\omega}$ and $Z^\infty_{\ell m\omega}$ determine the gravitational energy fluxes emitted at infinity and through the horizon [67, 69]:

$$\dot{E}^\infty = \sum_{lm} \frac{|Z^\infty_{\ell m\omega}|^2}{4\pi(m\Omega)^2} \,, \tag{18}$$

$$\dot{E}^H = \sum_{lm} \frac{\alpha_{\ell m} |Z^H_{\ell m\omega}|^2}{4\pi(m\Omega)^2} \,, \tag{19}$$

where

$$\alpha_{\ell m} = \frac{256(2Mr_+)^5 k(k^2 + 4\varpi^2)(k^2 + 16\varpi^2)(m\Omega)^3}{|c_{\ell m}|^2} \,, \tag{20}$$

with $\varpi = \sqrt{M^2 - a^2}/(4Mr_+)$ and

$$\begin{aligned} |c_{\ell m}|^2 = & [(\lambda+2)^2 + 4ma(m\Omega) - 4a^2(m\Omega)^2] \\ & \times [\lambda^2 + 36ma(m\Omega) - 36a^2(m\Omega)^2] \\ & + (2\lambda+3)[96a^2(m\Omega)^2 - 48ma(m\Omega)] \\ & + 144(m\Omega)^2(M^2 - a^2) \,. \end{aligned} \tag{21}$$

For circular equatorial orbits, the angular momentum fluxes are related to the energy fluxes at infinity and at the horizon by $\dot{J}^{\infty,H} = \dot{E}^{\infty,H}/\Omega$.

In the BH case, the total energy flux emitted by a point particle in a circular equatorial orbit with orbital angular frequency Ω is

$$\dot{E}(\Omega) = \dot{E}^\infty(\Omega) + \dot{E}^H(\Omega) \,, \tag{22}$$

where $\dot{E}^\infty(\Omega)$ and $\dot{E}^H(\Omega)$ are defined in Eqs. (18) and (19), respectively.

2. Horizonless case

As discussed above, we assume that, at least in the exterior of the central object, General Relativity is a valid approximation. Therefore for $r > r_0$ the perturbations equations are the

same as in the Kerr BH case, and possible corrections can be incorporated in the boundary conditions for the gravitational radiation at the effective radius.

The physical interpretation of the inner boundary condition is more evident by adopting the Detweiler's function [70]

$$X_{\ell m\omega} = \frac{\left(r^2+a^2\right)^{1/2}}{\Delta}\left[\alpha(r)\, R_{\ell m\omega} + \beta(r)\Delta^{-1}\frac{dR_{\ell m\omega}}{dr}\right], \tag{23}$$

where $\alpha(r), \beta(r)$ are certain radial functions [4, 70]. Indeed, since any signal is totally absorbed, in the BH case the physical solution is a purely ingoing wave near the horizon,

$$X_{\ell m\omega} \sim e^{-ikr_*} \quad \text{as } r_* \to -\infty\,, \tag{24}$$

In the case of an ECO, the solution near the surface ($r \sim r_0$) is more involved and depends also on the value of ϵ [21]. Assuming $\epsilon \ll 1$, the effective potential in the Teukolsky's equation is constant near the surface, $V \approx -k^2$, so that the perturbation is a superposition of ingoing and outgoing waves at the ECO radius

$$X_{\ell m\omega} \sim A_{\rm in}e^{-ikr_*} + A_{\rm out}e^{ikr_*} \quad \text{as } r_* \to r_*^0\,, \tag{25}$$

where $r_*^0 \equiv r_*(r_0)$. One can therefore define the surface reflectivity of the ECO as [4]

$$\mathcal{R}(\omega) = \frac{A_{\rm out}}{A_{\rm in}}e^{2ikr_*^0}\,. \tag{26}$$

Perfectly reflecting objects have $|\mathcal{R}(\omega)|^2 = 1$, i.e., $\mathcal{R}(\omega) = e^{i\psi(\omega)}$ for an arbitrary (real) frequency-dependent phase ψ. Two notable examples of perfectly-reflecting boundary conditions are

$$\begin{cases} X_{\ell m\omega}(r_0) = 0 & \text{Dirichlet, } \mathcal{R} = -1 \\ dX_{\ell m\omega}(r_0)/dr_* = 0 & \text{Neumann, } \mathcal{R} = 1 \end{cases}, \tag{27}$$

corresponding to $\psi = \pi$ and $\psi = 0$, respectively. In general, a partially absorbing compact object is described by

$$\left.\frac{dX_{\ell m\omega}/dr_*}{X_{\ell m\omega}}\right|_{r_0} = -ik\frac{1-\mathcal{R}(\omega)}{1+\mathcal{R}(\omega)}\,, \tag{28}$$

which reduces to the BH boundary condition when $\mathcal{R} = 0$.

In the ECO case, the solutions of the homogeneous Teukolsky's equation are such that the 'up' modes have the same asymptotics as in Eq. (11), whereas the 'in' modes have the following asymptotics

$$R^{\rm in}_{\ell m\omega} \sim \begin{cases} B'^{\rm trans}_{\ell m\omega}\Delta^2 e^{-ikr_*} + C'^{\rm up}_{\ell m\omega}e^{ikr_*} & \text{as } r_* \to r_*^0 \\ r^3 B'^{\rm ref}_{\ell m\omega}e^{i\omega r_*} + r^{-1}B'^{\rm inc}_{\ell m\omega}e^{-i\omega r_*} & \text{as } r_* \to +\infty \end{cases}, \tag{29}$$

where

$$B'^{\rm trans}_{\ell m\omega} = B^{\rm trans}_{\ell m\omega} + c_1 C^{\rm ref}_{\ell m\omega}\,, \tag{30}$$
$$C'^{\rm up}_{\ell m\omega} = c_1 C^{\rm up}_{\ell m\omega}\,, \tag{31}$$
$$B'^{\rm ref}_{\ell m\omega} = B^{\rm ref}_{\ell m\omega} + c_1 C^{\rm trans}_{\ell m\omega}\,, \tag{32}$$
$$B'^{\rm inc}_{\ell m\omega} = B^{\rm inc}_{\ell m\omega}\,, \tag{33}$$

and the coefficient c_1 is determined by imposing the boundary condition in Eq. (28) with

$$R_{\ell m\omega} = R^{\rm in}_{\ell m\omega} + c_1 R^{\rm up}_{\ell m\omega}\,. \tag{34}$$

The inhomogeneous solution of the Teukolsky's function is derived as in Eq. (12), with $R^{\rm in}_{\ell m\omega}$ as in Eq. (29) and $R^{\rm up}_{\ell m\omega}$ as in Eq. (11), and has the following asymptotic behavior

$$R_{\ell m\omega} \sim \begin{cases} Z^H_{\ell m\omega}\Delta^2 e^{-ikr_*} + Z^{\rm out}_{\ell m\omega}e^{ikr_*} & \text{as } r_* \to r_*^0 \\ Z^\infty_{\ell m\omega} r^3 e^{i\omega r_*} & \text{as } r_* \to +\infty \end{cases}, \tag{35}$$

where

$$Z^{\rm out}_{\ell m\omega} = \frac{B'^{\rm ref}_{\ell m\omega}}{B'^{\rm trans}_{\ell m\omega}}Z^H_{\ell m\omega}\,, \tag{36}$$

and the energy flux emitted outside the ECO radius is [67]

$$\dot{E}^{\rm out} = \sum_{lm}\frac{\omega}{4\pi k(2r_+/M)^3(k^2+4\varpi^2)}|Z^{\rm out}_{\ell m\omega}|^2\,, \tag{37}$$

In the ECO case, the energy flux emitted at infinity is defined in Eq. (18), whereas the energy flux emitted at the ECO radius is defined as

$$\dot{E}^{\rm radius} = \dot{E}^H - \dot{E}^{\rm out}\,, \tag{38}$$

which reduces to $\dot{E}^{\rm radius} = \dot{E}^H$ in the case of $\mathcal{R} = 0$. When $|\mathcal{R}(\omega)|^2 = 1$, the outgoing flux is equal to the ingoing flux at the ECO radius and $\dot{E}^{\rm radius} = 0$, as expected from fully reflecting boundary conditions.

In the ECO case, the total energy flux emitted by a point particle in a circular equatorial orbit is

$$\dot{E}(\Omega) = \dot{E}^\infty(\Omega) + \dot{E}^{\rm radius}(\Omega)\,, \tag{39}$$

where $\dot{E}^\infty(\Omega)$ and $\dot{E}^{\rm radius}(\Omega)$ are defined in Eqs. (18) and (38), respectively.

C. Adiabatic evolution and waveform

In an EMRI the radiation-reaction time scale is much longer than the orbital period so – at the first order in the mass ratio – the orbital parameters can be evolved using an adiabatic expansion [71]. For a particle in a circular equatorial and corotating orbit, the evolution of the orbital angular frequency Ω and the orbital phase ϕ are governed by

$$\dot{\Omega} = -\left(\frac{dE_b}{d\Omega}\right)^{-1}\dot{E}(\Omega)\,, \tag{40}$$
$$\dot{\phi} = \Omega\,, \tag{41}$$

where E_b is the binding energy of the system

$$E_b = \mu\frac{1-2v^2+\chi v^3}{\sqrt{1-3v^2+2\chi v^3}}\,, \tag{42}$$

with $\chi = a/M$, $v \equiv \sqrt{M/r}$, r is the orbital radius which is related to the orbital angular frequency via Eq. (9), and $\dot{E}(\Omega)$ is the total energy flux defined in Eqs. (22) and (39) in the BH and in the ECO case, respectively.

Equations (40), (41) can be solved with some initial conditions $\Omega(t = 0) = \Omega_0$ and (without loss of generality) $\phi(t = 0) = 0$. The GW phase of the dominant mode is related to the orbital phase by $\phi_{\rm GW} = 2\phi$. The GW dephasing accumulated up to a certain time between the BH case and ECO case is computed as [31]

$$\Delta\phi(t) = \phi^{\rm BH}_{\rm GW}(t) - \phi^{\rm ECO}_{\rm GW}(t)\,. \tag{43}$$

The emitted waveform is computed from the Weyl scalar at infinity and reads [27, 72]

$$h_+ - ih_\times = -\frac{2}{\sqrt{2\pi}}\frac{\mu}{D}\sum_{\ell,m}\frac{Z^\infty_{\ell m\omega}(t)}{[m\Omega(t)]^2}e^{im\left(\Omega(t)r^D_* - \phi(t)\right)} \times\ {}_{-2}S_{\ell m\omega}(\vartheta, t)e^{im\varphi}\,, \tag{44}$$

where D is the source luminosity distance from the detector, $r^D_* \equiv r_*(D)$, and (ϑ, φ) identify the direction, in Boyer-Lindquist coordinates, of the detector in a reference frame centered at the source. Since the initial phase is degenerate with the azimuthal direction, we simply rescale the initial phase as $\varphi \equiv \phi(t = 0)$.

Note that, regardless of its reflectivity, an ultracompact object can efficiently trap radiation within its photon sphere [11, 12, 73]. If radiation is trapped for enough time, it can contribute to the energy balance used to evolve the orbit adiabatically, thus mimicking the effect of a horizon even in the absence of dissipation within the object. However, this energy trapping at the photon sphere is not effective for a particle in circular orbit if [26, 31]

$$\epsilon \gg \exp\left(-\frac{5\sqrt{1-\chi^2}}{64q\left(1+\sqrt{1-\chi^2}\right)}\right)\,. \tag{45}$$

Owing to the mass-ratio dependence, this condition is always satisfied in the EMRI limit ($q \lesssim 10^{-5}$) for any realistic value of ϵ and χ. Therefore for an EMRI the only way to absorb radiation near the central ECO is by dissipating in its interior, i.e. when $|\mathcal{R}|^2 < 1$.

Spinning horizonless Kerr-like objects are affected by the so-called ergoregion instability [74, 75] when spinning sufficiently fast [3, 4, 76–78]. In this case the central object would spin down reaching a stable configuration. The instability time scale can be shorter than the orbital period and would affect the dynamics of the point particle. Since unstable solutions should not form in the first place or anyway do not live enough to form an EMRI, we shall focus our analysis on stable Kerr-like horizonless objects only. Stability is reached by assuming partially absorbing compact objects ($\mathcal{R} < 1$) [4] or specific models for the frequency-dependent reflectivity $\mathcal{R}(\omega)$ [53], so that the net absorption of the relevant frequencies is higher than the superradiant amplification that leads to the ergoregion instability [3, 4].

Finally, note that horizonless compact objects contain low-frequency modes in their spectrum, which are associated with long-lived quasibound states efficiently confined within the object photon sphere [3, 4, 21, 73]. At variance with the BH case, these low-frequency modes can be excited during a quasicircular inspiral when the orbital frequency equals the QNM frequency, leading to resonances in the fluxes [49–52]. As discussed in Sec. III, these resonances can be very narrow and require very high resolution in order to resolve them.

D. Overlap

Although the dephasing $\Delta\phi$ between two different waveforms ($h_1(t)$ and $h_2(t)$) is a useful and quick measure to estimate the impact of different effects, a somewhat more reliable and robust measure to assess the measurability of any deviation from a standard reference signal is given by the overlap:

$$\mathcal{O}(h_1|h_2) = \frac{\langle h_1|h_2\rangle}{\sqrt{\langle h_1|h_1\rangle\,\langle h_2|h_2\rangle}}\,, \tag{46}$$

where the inner product $\langle h_1|h_2\rangle$ is defined by

$$\langle h_1|h_2\rangle = 4\Re\int_0^\infty \frac{\tilde{h}_1\tilde{h}_2^*}{S_n(f)}df\,, \tag{47}$$

and $S_n(f)$ is the GW detector noise power spectral density, and the tilded quantities and the star stand for the Fourier transform and complex conjugation, respectively. For the power spectral density we adopted the LISA curve of Ref. [79] adding the contribution of the confusion noise from the unresolved Galactic binaries for a one year mission lifetime. Since the waveforms are defined up to an arbitrary time and phase shift, it is also necessary to maximize the overlap in Eq. (46) over these quantities. In practice this can be done by computing [80]

$$\mathcal{O}(h_1|h_2) = \frac{4}{\sqrt{\langle h_1|h_1\rangle\,\langle h_2|h_2\rangle}}\max_{t_0}\left|\mathcal{F}^{-1}\left[\frac{\tilde{h}_1\tilde{h}_2^*}{S_n(f)}\right](t_0)\right|\,, \tag{48}$$

where $\mathcal{F}^{-1}[g(f)](t) = \int_{-\infty}^{+\infty} g(f)e^{-2\pi ift}df$ is the inverse Fourier transform. The overlap is defined such that $\mathcal{O} = 1$ indicates a perfect agreement between two waveforms. It is also customary to define the mismatch $\mathcal{M} \equiv 1 - \mathcal{O}$.

E. Numerical procedure

We have studied the dynamics of a point particle in a circular equatorial orbit around a Kerr-like ECO by adapting the frequency-domain Teukolsky code originally developed in Refs. [81–84]. In particular, the solutions to the homogeneous Teukolsky's equation are calculated via the numerical Mano-Suzuki-Takasugi method [68, 85–87]. The use of this method gives full analytical control over the boundary conditions, making it perfectly suited for our purpose. We have modified the (frequency-dependent) boundary conditions at

$r = r_0$ in terms of $\mathcal{R}$ and ϵ as discussed in Sec. II B, computed the energy and angular-momentum fluxes at infinity and through the object's surface, and finally evolved the quasi-circular orbit adiabatically by integrating Eqs. (40) and (41).

Our algorithm is the following:

1. Choose the intrinsic parameters of the binary, namely the central mass M, the mass ratio $q \ll 1$, the primary spin χ, the reflectivity $\mathcal{R}(\omega)$ and the compactness of the central object and the initial orbital radius.

2. For a given $\ell = m$ mode, produce the data for a bound orbit with orbital radius r and compute the energy fluxes in the cases of a central BH and a central ECO, respectively.

3. Loop on the orbital radii with an equally spaced (radial) grid starting from the ISCO radius to $r = 10M$.

4. Find the local maxima and minima in the energy fluxes at infinity for a central ECO. If present, these extrema bracket resonances in the flux, which should be resolved by increasing the grid resolution. Note that the initial equally-spaced grid in the orbital radii needs to be dense enough to find local maxima and minima. For this reason, we set the initial discretization in the orbital radii to be $0.003M$.

5. Refine the grid on the orbital radii around local maxima and minima through bisection until a target accuracy is reached. The refinement of the grid stops either when the difference between two subsequent orbital radii is $< 10^{-5}M$ or when the difference in the energy fluxes of two subsequent points is $< 10^{-5}q^2$.

6. For a given ℓ and each $m = \ell - 1, ..., 1$ loop on the orbital radii with an equally spaced grid from the ISCO radius. The loop stops when the total energy flux of the central BH is smaller than 10^{-6} times the total energy flux of the central BH for the $\ell = m$ dominant mode.

7. For a given ℓ and each $m = \ell - 1, ..., 1$ repeat steps 4 and 5.

8. For the harmonic index $\ell = 2, ..., \ell_{\rm max} = 12$ repeat the steps 2 to 7.

9. For each ℓ, m mode, interpolate the total energy flux as function of the orbital angular frequency.

10. Sum over the modes and integrate Eqs. (40) and (41) to compute the orbital phase both in the BH and in the ECO cases. The initial condition on the orbital angular frequency is $\Omega_0 = \Omega(r = 10M)$ and the integration stops at the inspiral-plunge transition frequency [88] $\Omega(t_{\rm max}) = \Omega(r = r_{\rm ISCO} + 4q^{2/3})$.

The gravitational waveform is computed via Eq. (44), where for the modes with negative m we make use of the following symmetries

$$Z^{\infty}_{\ell -m\omega} = (-1)^{\ell} \left(Z^{\infty}_{\ell m\omega}\right)^* , \tag{49}$$

$${}_{-2}S_{\ell -m\omega}(\vartheta) = (-1)^{\ell}\, {}_{-2}S_{\ell m\omega}(\pi - \vartheta) . \tag{50}$$

For each ℓ, m mode the asymptotic amplitudes at infinity and the spin-weighted spheroidal harmonics are interpolated functions of the time-dependent orbital angular frequency. The waveform is constructed by summing over the modes with $\ell \leq 4$ and $-\ell \leq m \leq \ell$. In the cases of small reflectivity ($|\mathcal{R}|^2 \leq 10^{-6}$) the waveform is constructed by summing over the ℓ, m modes until $\ell = 5$.

We tested our code by reproducing standard results for the Kerr BH case [27–30]. Furthermore, we reproduced the results of Ref. [31] for a Kerr-like ECO using the same assumptions, i.e., we considered the Kerr BH case and artificially impose that only a fraction $(1-|\mathcal{R}|^2)$ of the radiation is absorbed at the surface.

The fractional truncation error of the code is estimated in the dephasing as $\Delta^{\rm tr} = 1 - \Delta\phi_{\ell_{\rm max}+1}(t_f)/\Delta\phi_{\ell_{\rm max}}(t_f)$, where the energy fluxes are truncated at $\ell_{\rm max} = 12$ and t_f is the time at which the orbital radius is $r = r_{\rm ISCO} + 4q^{2/3}$. For a reference compact object with $\chi = 0.9$, $|\mathcal{R}|^2 = 0.9$, $\epsilon = 10^{-10}$, and $q = 3 \times 10^{-5}$, we find $\Delta^{\rm tr} = 2 \times 10^{-5}$.

III. RESULTS

In this section we present our main results. In Secs. III A, III B, III C we consider an agnostic model with generic values of ϵ and $\mathcal{R}$. In Sec. III D, we shall specialize to the Boltzmann reflectivity model of Ref. [53].

A. Energy fluxes and resonances

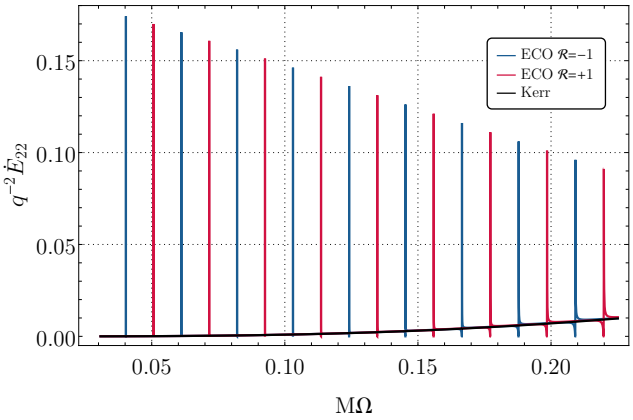

FIG. 1. Total energy flux of the $\ell = m = 2$ mode as a function of the orbital angular frequency for a point particle in quasicircular equatorial orbit from $r = 10M$ to $r = r_{\rm ISCO}$. We compare the case of a central Kerr BH with spin $\chi = 0.9$ to the case of a central ECO with a perfectly reflecting surface ($|\mathcal{R}|^2 = 1$), $\chi = 0.9$, and $\epsilon = 10^{-10}$. In the latter case the flux is resonantly excited when the orbital frequency matches the low-frequency QNMs of the ECO.

Let us start by discussing the modified energy flux in the case of a spinning horizonless compact object. As a repre-

sentative example, Fig. 1 shows the $\ell = m = 2$ component of the total energy flux as a function of the orbital frequency for $\epsilon = 10^{-10}$, $\chi = 0.9$, and for two choices (Dirichlet and Neumann) of perfectly-reflecting boundary conditions. As expected, the flux is resonantly excited when the frequency matches the low-frequency QNMs of the central ECO ($\Omega = \omega_R/m$). This is a striking difference with respect to the BH case, since the Kerr QNMs have higher frequencies and cannot be resonantly excited by quasicircular inspirals. In the small-ϵ limit, the Dirichlet and Neumann modes are described by [4]

$$\omega_R \sim -\frac{\pi(p+1)}{2|r_*^0|} + m\Omega_H \,, \tag{51}$$

$$\omega_I \sim -\frac{\beta_l}{|r_*^0|}\left(\frac{2Mr_+}{r_+ - r_-}\right)\left[\omega_R(r_+ - r_-)\right]^{2l+1}(\omega_R - m\Omega_H) \,, \tag{52}$$

where $r_\pm = M \pm \sqrt{M^2 - a^2}$, $\sqrt{\beta_l} = \frac{(l+2)!(l-2)!}{(2l)!(2l+1)!!}$, and p is an odd (even) integer for Neumann (Dirichlet) modes. As shown in Fig. 1, for fixed χ and ϵ the modes are equispaced with $\Delta\omega_R = \pi/|r_*^0|$, whereas consecutive Dirichlet and Neumann mode frequencies are separated by half this width. The difference between consecutive resonances scales as $\Delta\omega_R \sim |\log\epsilon|^{-1}$, therefore the resonances are denser in the $\epsilon \to 0$ limit.

Interestingly, the resonances appear at the same frequencies in all the individual fluxes: $\dot{E}^\infty$, $\dot{E}^H$, and $\dot{E}^{\rm out}$. This is due to the fact that the QNMs are associated to the poles of the Wronskian appearing in each solution of the Teukolsky's equation. However, when $|\mathcal{R}|^2 = 1$ the fluxes $\dot{E}^H$ and $\dot{E}^{\rm out}$ are exactly equal to each other since in this case $\dot{E}^{\rm radius} = 0$. Therefore for the perfectly reflecting case resonances appear only in the flux at infinity.

Equation (52) shows that $\omega_I \ll \omega_R$, which implies that the resonances are typically very narrow and hard to resolve [49, 51, 52]. The energy flux across a single resonance is very well fitted by a forced harmonic oscillator model [89]

$$\frac{\dot{E}_{\rm ECO}}{\dot{E}_{\rm BH}} = \frac{[(1-b)(m\Omega)^2 - \omega_R^2 - \omega_I^2]^2 + (2m\Omega\omega_I)^2}{(m\Omega - \omega_R^2 - \omega_I^2)^2 + (2m\Omega\omega_I)^2} \,, \tag{53}$$

where $b = 1 - (\Omega_{\rm max}/\Omega_{\rm min})^2$, and $\Omega_{\rm max}$ and $\Omega_{\rm min}$ are the orbital angular frequencies of the maximum and the minimum of each resonance. The width of each resonance in the orbital frequency scales as $\delta\Omega \sim \omega_I$ [51], where $\omega_I \sim \omega_R^{2l+2}$ from Eq. (52). It follows that the width of the resonances increases with the orbital angular frequency as shown in Fig.1. In the nonspinning and perfectly reflecting case we recover the results of Ref. [51], namely that low-frequency resonances do not contribute significantly to the GW phase (see Appendix A). However, as discussed below, for highly spinning compact objects, the ISCO frequency occurs at higher frequencies with respect to the nonspinning case and higher-frequency resonances can be efficiently excited, contributing a significant dephasing with respect to the BH case.

The system shown in Fig. 1 is purely indicative, since for this choice of the parameters the central ECO is unstable and would tend to spin down on short time scales [3, 4]. This is also shown by the fact that ω_I in Eq. (52) is positive ($\omega_R < m\Omega_H$), as expected due to the ergoregion instability. Stable solutions require either smaller values of the spin or partial absorption [3, 4]. In all these cases the resonances are less evident, as shown in Fig. 2, where we considered a model with $|\mathcal{R}|^2 = 0.9$, a value that guarantees stability for $\chi = 0.9$ [4].

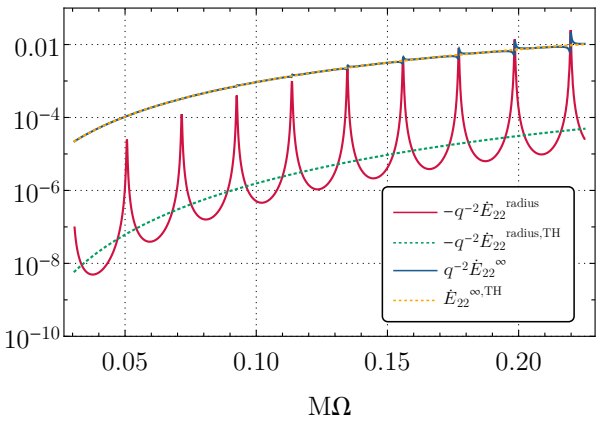

FIG. 2. Energy fluxes emitted at the radius and at infinity by a point particle around a central ECO with $\chi = 0.9$, $\epsilon = 10^{-10}$, and $\mathcal{R} = \sqrt{0.9}$ for the $\ell = m = 2$ mode. The fluxes are compared with those of Ref. [31] in which the effect of the ECO was accounted for by simply removing a fraction ($|\mathcal{R}|^2$ of the tidal heating (TH) from a standard Kerr EMRI flux.

Several comments are in order. First of all, also for a smaller reflectivity we observe resonances in $\dot{E}^\infty$ as in the perfectly-reflecting case of Fig. 1: in this case they are less peaked but, as shown below, could still have a sufficiently large width to be efficiently excited. Second, the same resonant frequencies appear also in $\dot{E}^{\rm radius}$. This is due to the fact that for $|\mathcal{R}| < 1$ the fluxes $\dot{E}^H$ and $\dot{E}^{\rm out}$ do not exactly compensate each other, leaving a net flux at the ECO radius that can be resonantly excited. Near the resonances and at high frequencies, this flux is comparable to $\dot{E}^\infty$ and contributes significantly to the GW phase.

Finally, in Fig. 2 we also show the fluxes at infinity and at the ECO radius computed with the simplified model of Ref. [31], i.e., by artificially removing a fraction ($|\mathcal{R}|^2$) of the tidal heating from a standard EMRI flux around a central Kerr BH. We observe that the energy flux at infinity in this case is similar to the exact result, except for the presence of the resonances (which are absent in the model of Ref. [31]). On the other hand, the energy flux at the radius can change significantly. Due to the presence of the resonances, $\dot{E}^{\rm radius}$ computed in Ref. [31] is, roughly speaking, a sort of averaged value of the exact result. The latter is modulated by the presence of resonances, which can be as high as the flux at infinity.

In Fig. 3 we show the difference between the total energy flux of the $\ell = m = 2$ mode in the horizonless case with respect to the BH case. In particular, the left panel shows the absolute value of this quantity in a logarithmic scale, in order to appreciate the relatively small numbers involved. In

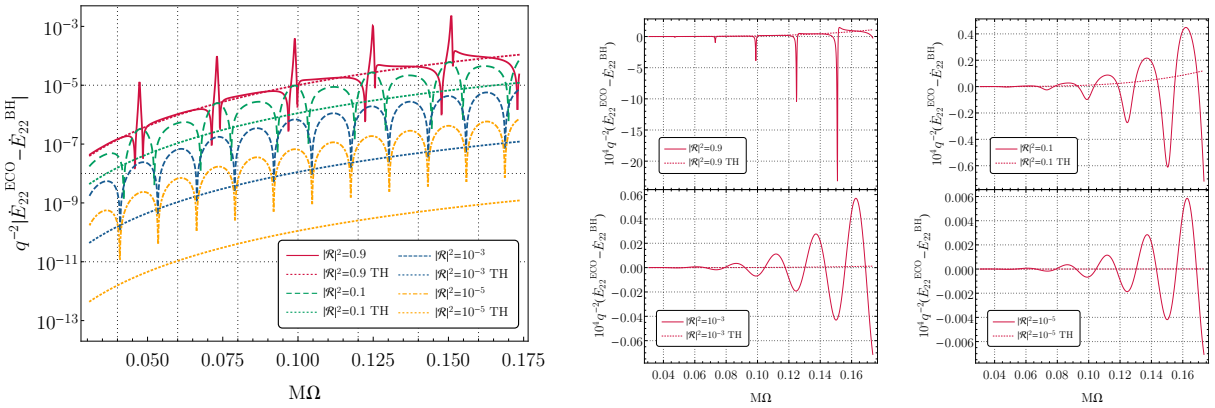

FIG. 3. Difference between the total energy flux of the $\ell = m = 2$ mode in the ECO case with respect to the BH case. Left panel: absolute value of the difference for $\chi = 0.8$, $\epsilon = 10^{-10}$, and several values of the reflectivity. The dotted lines are the estimated differences in the total energy flux due to the absence of tidal heating relative to the BH case as in Ref. [31]. Right panels: same as in the left panel but without the absolute value and in a linear scale, to appreciate the change of sign during the oscillations associated with the resonances.

the right panel grid, instead, we show the same quantity in a linear scale and without the absolute value, to appreciate the change of sign during the oscillations.

For $|\mathcal{R}|^2 \approx 1$ the differences between the consistent model and the model of Ref. [31] are due to two factors: the excitation of resonances and the (subleading) fact that the flux computation in the consistent model is more accurate, since it accounts for the fraction of the GWs that are reflected by the object and make their way to infinity rather than being reabsorbed by the particle, as implicitly assumed in [31]. Furthermore, for smaller values of the reflectivity, the difference between our consistent model and the simplified one is even more important. In this case the resonances are suppressed in amplitude but still appear in the total energy flux with a larger width, as shown in the left panel of Fig. 3. The right panel grid in Fig. 3 shows the oscillatory trend of the total energy flux in the horizonless case compared to the energy flux in Ref. [31] for small reflectivities. The amplitude of the oscillations increases with the orbital angular frequency and descreases with the reflectivity. These oscillations are related to the resonances and, as we shall see in Sec. III B, they can contribute significantly to the GW phase also for small values of $\mathcal{R}$.

Interestingly, when the superradiance condition, $\Omega < \Omega_H$, is met, the flux at the radius can be negative, due to superradiant energy and angular-momentum extraction from the central object [9]. Since $\dot{E}^{\rm radius}$ and $\dot{E}^{\infty}$ have the opposite sign, it is interesting to check if they can exactly compensate each other at some given frequency, giving rise to a total zero flux and hence to "floating" orbits [90, 91]. As clear from Fig. 2, limiting to the case of $\ell = m = 2$ mode only such orbits would exist. However, they exist only near high-frequency resonances, where $\dot{E}^{\rm radius}$ (which is typically subdominant) can be as large (in absolute value) as $\dot{E}^{\infty}$. When including the contribution of $\ell > 2$ multipoles, we find that the total flux at infinity is larger than the flux at the radius, because modes with different (ℓ, m) are resonantly excited at different frequencies. The net result is that the total flux, $\dot{E}^{\infty} + \dot{E}^{\rm radius}$, is overall positive and the orbit shrinks during the adiabatic evolution.

B. Dephasing

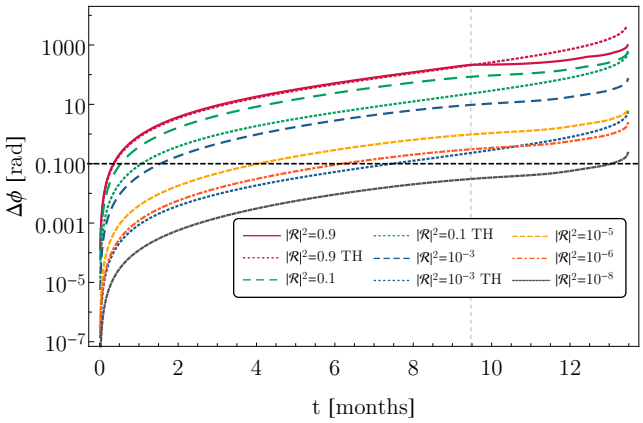

FIG. 4. GW dephasing between the BH and the ECO case as a function of time for $\chi = 0.8$, $q = 3 \times 10^{-5}$, $\epsilon = 10^{-10}$, and several values of the reflectivity. The dotted lines show the dephasing due to the absence of tidal heating relative to the BH case as in Ref. [31]. The vertical dashed line denotes the time corresponding to a resonant orbital frequency. The horizontal line is a reference value $\Delta\phi = 0.1$ rad [92, 93].

With the total flux at hand until $\ell_{\rm max} = 12$, we now move to study the dephasing between a horizonless compact object and the standard Kerr case. This is shown in Fig. 4 for a fiducial binary with $M = 10^6 M_\odot$, $\mu = 30 M_\odot$, $\chi = 0.8$, and $\epsilon = 10^{-10}$. We analyze different values of the reflectivity $|\mathcal{R}|^2$ and for each of them we compare our exact result

with that of the model adopted in Ref. [31]. As expected, the dephasing increases monotonically in time (except possibly when a resonance is crossed, in which case the dephasing can have an antispike and decreases near the resonant frequency, see Appendix B) and also as a function of the reflectivity. When $|\mathcal{R}|^2 \approx 1$, the difference with respect to the model adopted in Ref. [31] is small until the inspiral moves across a resonance. In particular for $|\mathcal{R}|^2 = 0.9$, the dephasing with respect to our exact results deviates from the dephasing due to the absence of tidal heating at $t = 9.47\,\mathrm{months}$ (marked in Fig. 4 by a dashed vertical line) due to the presence of a $\ell = m = 2$ resonance at $M\Omega = 0.0473$ with $M\omega_I = -4.22 \times 10^{-5}$. Subsequent resonances are excited at later times.

The simplified model of Ref. [31] and the exact result differ significantly for small reflectivities even if the resonances are less evident. This is due to a number of factors: the energy fluxes at the ECO radius and at infinity display some differences in the two models due to the fact that a fraction of energy is reflected by the object and leaves the system; moreover, both fluxes (at the radius and at infinity) can be resonantly excited only in our consistent model and these resonances contribute significantly to the GW phase for intermediate values of $\mathcal{R}$. The dephasing in the consistent model is always larger than the dephasing with tidal heating only (for very small values of $\mathcal{R}$, the two models differ but both produce a tiny dephasing, as expected). The dephasing depends mildly on the compactness of the object, see Appendix B for an analysis of this contribution.

C. Overlap

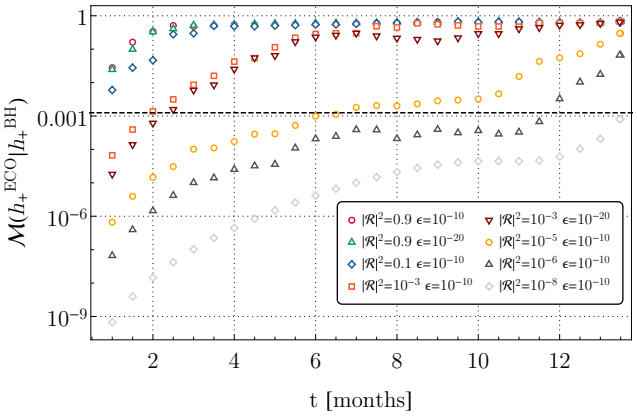

FIG. 5. Mismatch between the plus polarization of the waveforms with a central ECO and a central BH as a function of time, for $\chi = 0.8$, $q = 3 \times 10^{-5}$ and several values of the reflectivity.

In Fig. 5 we show the mismatch $\mathcal{M} \equiv 1 - \mathcal{O}$ between the waveforms in the ECO case and in the Kerr case with the same mass and spin for various values of $\mathcal{R}$ and two choices of ϵ.

As clear from the plot, the value of ϵ does not affect the mismatch significantly as long as $\epsilon \ll 1$. Consistently with dephasing presented above, the mismatch is larger for the consistent model, especially at small reflectivity, as can be appreciated by comparing our Fig. 5 with the corresponding plot in Ref. [31]. As a useful rule of thumb, two waveforms can be considered indistinguishable for parameter estimation purposes if $\mathcal{M} \lesssim 1/(2\rho^2)$, where ρ is the signal-to-noise ratio of the true signal [92, 94]. For an EMRI with $\rho \approx 20$ (resp., $\rho \approx 100$) one has $\mathcal{M} \lesssim 10^{-3}$ (resp., $\mathcal{M} \lesssim 5 \times 10^{-5}$). In Fig. 5 the more conservative threshold $\mathcal{M} = 10^{-3}$ is denoted with a dashed horizontal line. Exceeding this threshold is a necessary but not sufficient condition for a deviation to be detectable. This level of mismatch is quickly exceeded after less than one year of data even for small values of the reflectivity. For example, for the fiducial case considered in Fig. 5 ($\chi = 0.8$, $M = 10^6 M_\odot$ and $\mu = 30 M_\odot$), and assuming $\rho = 20$, the threshold is exceeded after roughly one year unless

$$|\mathcal{R}|^2 \lesssim 10^{-8}\,. \tag{54}$$

Note however that the above bound is solely based on the mismatch calculation and does not take into account, e.g., correlations with other waveform parameters. A rigorous parameter estimation is necessary to derive an accurate projected upper bound (in the case of no detection). This interesting analysis goes beyond our scope and is left for future work.

D. A case study: EMRI constraints on Boltzmann reflectivity

Although so far we have considered only the case in which $|\mathcal{R}|^2 = \mathrm{const}$, an advantage of our framework is that the reflectivity coefficient can be a generic complex function of the model's parameters and of the frequency. We now consider a specific model for the ECO reflectivity. In particular, we shall assume a model recently proposed to describe quantum BH horizons, which gives rise to "Boltzmann" reflectivity [53, 95]

$$\mathcal{R}(\omega) = e^{-\frac{|k|}{2T_H}}\,, \tag{55}$$

where $T_H = \frac{r_+ - r_-}{4\pi(r_+^2 + a^2)}$ is the Hawking temperature of a Kerr BH. In this model the reflectivity depends explicitly on the spin and on the frequency. Furthermore, it provides sufficient absorption to quench the ergoregion instability [53]. Note that Eq. (55) can also contain a phase term, which depends on the specific model and on the perturbation function on which the corresponding boundary condition is imposed [53, 63, 95]. For simplicity, here we shall neglect such phase term, which anyway would not affect our analysis. [3]

Figure 6 shows the dephasing (left panel) and the overlap (right panel) obtained in the Boltzmann reflectivity model as compared to the classical BH case. An interesting feature of

[3] Recently Refs. [63, 96] proposed an alternative model for the ECO reflectivity that is related to the tidal response of the ECO to external curvature perturbations. In this model the reflectivity contains extra terms that multiply the Boltzmann factor.

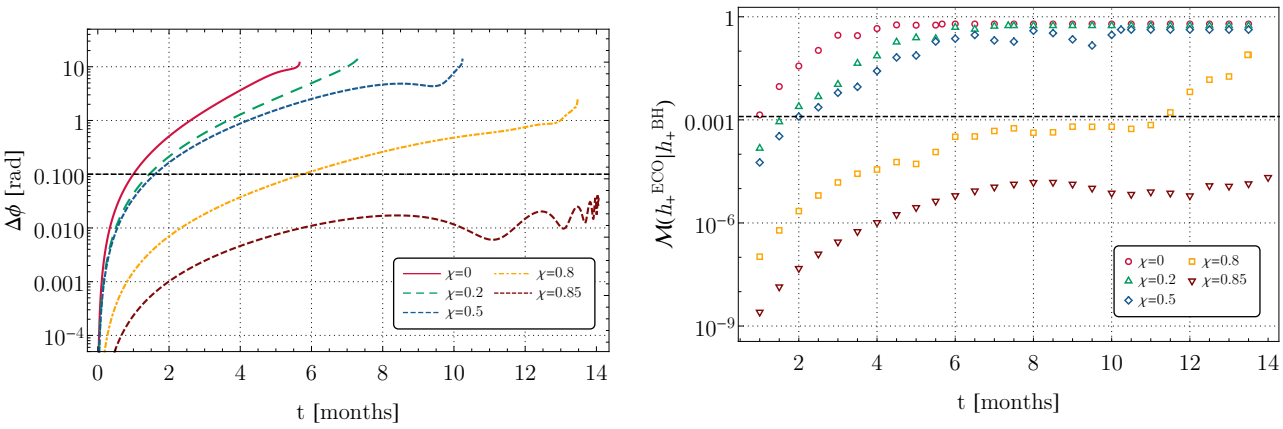

FIG. 6. Left: GW dephasing between the Kerr case and a quantum BH horizon with Boltzmann reflectivity [in Eq. (55)], $\epsilon = 10^{-10}$, $q = 3 \times 10^{-5}$ and various values of the spin, as a function of time. Right: Mismatch between the plus polarization of the waveform with a central quantum BH horizon with Boltzmann reflectivity and a central BH as a function of time for several values of the primary spin.

this model is that there is no free parameter that continuously connects it to the classical Kerr case, so there is a concrete chance to rule it out with observations, or to provide evidence for it. Interestingly, owing to its spin dependence, the Boltzmann reflectivity is much smaller at the relevant orbital frequencies when the central object is highly spinning. Therefore, as shown in Fig. 6, the dephasing and the mismatch with respect to the standard Kerr BH case are very small when $\chi \gtrsim 0.8$. The oscillatory trend in the dephasing is due to the contribution of high frequency resonances appearing at late times.

IV. CONCLUSION

EMRIs will be unparalleled probes of fundamental physics and unique sources for the LISA mission and evolved concepts thereof [46]. Developing a consistent model of partially absorbing ECO, we studied the signal emitted by a point particle in circular motion. The EMRI dynamics is affected by the modified boundary conditions at the object's surface, which give rise to modified tidal heating, modified fluxes, and resonant QNM excitations in a consistent fashion. We showed that the GW emission and orbital dynamics in the consistent model is quite rich: in addition to some quantitative differences with respect to the simplified model studied in Ref. [31], there are also qualitatively new features such as resonances that might give a relevant contribution to the GW phase in some regions of the parameter space. In principle, these resonances could also jeopardize detection if not suitable accounted for in the waveform.

Overall, we found that the already very stringent potential bounds derived in Ref. [31] can be further improved by some orders of magnitude by taking into account a consistent ECO model. These projected constraints suggest that EMRI could place the strongest bounds on the reflectivity of supermassive objects, orders of magnitude more stringent than those potentially coming from echo searches in the post-merger phase of comparable-mass coalescences [18, 19]. In particular, we showed that an EMRI detection is potentially sensitive to an effective reflectivity of the central supermassive object as small as $|\mathcal{R}|^2 \sim \mathcal{O}(10^{-8})$. As a reference, we remind that in the BH case the reflectivity is exactly zero and that for a neutron star it is practically unity, even when accounting for dissipation due to viscosity [2]. Furthermore, we showed that this unique sensitivity to small reflectivity coefficients can be used to constrain specific ECO models, such as those of quantum BH horizons featuring Boltzmann reflectivity [53, 95]. Our approach is general and the reflectivity coefficient can be an arbitrary complex function of the model parameters and of the frequency, so the same analysis can be applied to other specific ECO models, e.g. [63, 96].

However, the above conclusion is based on several simplifications that should be relaxed in future work. In particular, we focused on circular, equatorial orbits while EMRIs are expected to be eccentric and nonplanar, introducing two further parameters (the eccentricity and the Carter constant) in the description of the inspiral. Future work should also include leading-order self-force effects [97–99], which are needed for an accurate parameter estimation with EMRIs [71]. Both can be done with the minor adjustments of the code of Refs. [81–84] described here. Finally, the upper bounds estimated here are based on the overlap calculation, and therefore neglect possible correlations among the waveform parameters, which is particularly relevant for generic orbits and relatively small signal-to-noise ratio. From the parameter-estimation point of view, it is important to develop modified kludge waveforms to include ECO effects in a practical way or, more ambitiously, to perform accurate data analyses using exact waveforms (either using the Fisher-information matrix or, ideally, a Bayesian inference), extending recent work in the context of standard waveforms [100–102].

ACKNOWLEDGMENTS

The authors are grateful to Richard Brito, Sayak Datta, Simone Mastrogiovanni, and Gabriel Andres Piovano for useful discussions. Numerical computations were performed at the Vera cluster of the Amaldi Research Center funded by the MIUR program "Dipartimento di Eccellenza" (CUP: B81I18001170001). E. M. and P. P. acknowledge the financial support provided under the European Union's H2020 ERC, Starting Grant agreement no. DarkGRA–757480. We also acknowledge support under the MIUR PRIN and FARE programmes (GW- NEXT, CUP: B84I20000100001).

Appendix A: Dephasing in the nonspinning case

For completeness, here we show the dephasing in the case of a nonspinning, perfectly reflecting ECO relative to the Schwarzschild BH case for different values of the compactness parameters ϵ. Figure 7 shows that the dephasing essentially does not depend on ϵ and is not affected by the resonances, which in the nonspinning case are too narrow to be efficiently excited.

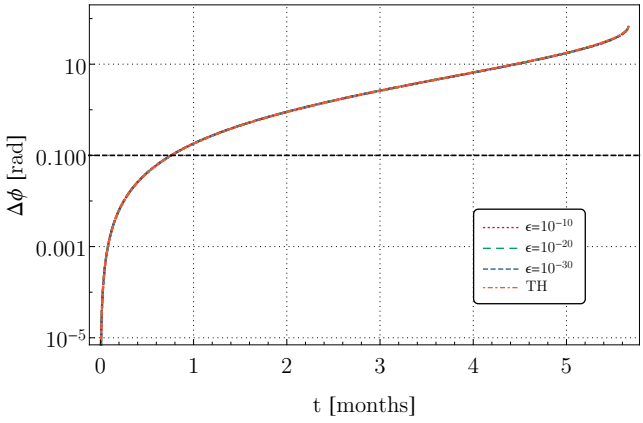

FIG. 7. Dephasing as a function of time in the case of a nonspinning, perfectly reflecting ECO relative to the Schwarzschild BH case for different values of the compactness parameters ϵ and $q = 3 \times 10^{-5}$. In this case the resonances in the flux at infinity do not contribute to the dephasing, which is well approximated by the simplified model of Ref. [31].

Appendix B: Fluxess and dephasing as function of the compactness

In Fig. 8 we show the difference between the ECO and Kerr BH total energy fluxes for several values of ϵ as a function of time. We note that, as ϵ decreases, more resonances appear and they also appear at lower frequencies. The first low-frequency resonances might give a large contribution to the phase since the orbital evolution is slower at low frequency and the particle can spend more time to move across the resonance. On the other hand, in our ECO model the width of each resonance is proportional to $\omega_I \sim \omega_R^{2l+2}$ and therefore low-frequency resonances are also more narrow. The two effects are competitive and the actual contribution of a resonance on the GW phase depends on the specific parameters of the configuration.

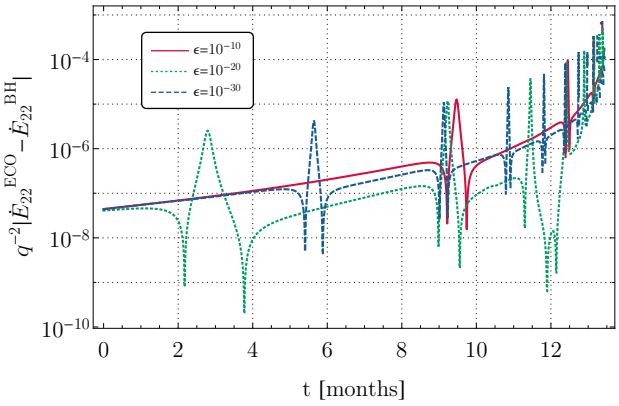

FIG. 8. Resonances in the $\ell = m = 2$ energy flux for an ECO with $\chi = 0.8$, $|\mathcal{R}|^2 = 0.9$ and several values of ϵ as a function of time.

Finally, in Fig. 9 we show the dephasing for some values of $|\mathcal{R}|^2$ and ϵ. The dependence on ϵ is mild, except for the possible excitation of the resonances, whose impact depends on the specific values of χ, ϵ and $\mathcal{R}$.

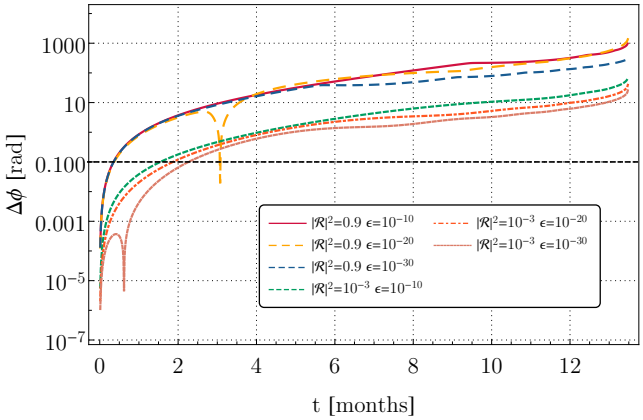

FIG. 9. GW dephasing between the BH and the ECO case as a function of time for $\chi = 0.8$, $q = 3 \times 10^{-5}$ and several values of ϵ.

[1] V. Cardoso and P. Pani, *Living Rev. Rel.* **22**, 4 (2019), arXiv:1904.05363.

[2] F.P. Esposito, ApJ **165**, 165 (1971).

[3] E. Maggio, P. Pani, and V. Ferrari, *Phys. Rev.* **D96**, 104047 (2017), arXiv:1703.03696.
[4] E. Maggio, V. Cardoso, S.R. Dolan, and P. Pani, (2018), arXiv:1807.08840.
[5] K.S. Thorne, R. Price, and D. Macdonald, *Black holes: the membrane paradigm*, edited by K.S. Thorne (Yale University Press, 1986).
[6] T. Damour, in *Proceedings of the Second Marcel Grossmann Meeting ofGeneral Relativity, edited by R. Ruffini, North Holland, Amsterdam, 1982 pp 587-608* (1982).
[7] E. Poisson, *Phys. Rev.* **D80**, 064029 (2009), arXiv:0907.0874.
[8] V. Cardoso and P. Pani, *Class. Quant. Grav.* **30**, 045011 (2013), arXiv:1205.3184.
[9] R. Brito, V. Cardoso, and P. Pani, *Lect. Notes Phys.* **906**, pp.1 (2015), arXiv:1501.06570.
[10] E. Maggio, P. Pani, and G. Raposo, (2021), arXiv:2105.06410.
[11] V. Cardoso, E. Franzin, and P. Pani, *Phys. Rev. Lett.* **116**, 171101 (2016), arXiv:1602.07309.
[12] V. Cardoso, S. Hopper, C.F.B. Macedo, C. Palenzuela, and P. Pani, *Phys. Rev.* **D94**, 084031 (2016), arXiv:1608.08637.
[13] J. Abedi, H. Dykaar, and N. Afshordi, *Phys. Rev.* **D96**, 082004 (2017), arXiv:1612.00266.
[14] Z. Mark, A. Zimmerman, S.M. Du, and Y. Chen, (2017), arXiv:1706.06155.
[15] V. Cardoso and P. Pani, *Nat. Astron.* **1**, 586 (2017), arXiv:1709.01525.
[16] H. Nakano, N. Sago, H. Tagoshi, and T. Tanaka, *PTEP* **2017**, 071E01 (2017), arXiv:1704.07175.
[17] Q. Wang and N. Afshordi, *Phys. Rev.* **D97**, 124044 (2018), arXiv:1803.02845.
[18] A. Testa and P. Pani, *Phys. Rev.* **D98**, 044018 (2018), arXiv:1806.04253.
[19] E. Maggio, A. Testa, S. Bhagwat, and P. Pani, *Phys. Rev. D* **100**, 064056 (2019), arXiv:1907.03091.
[20] J. Abedi, N. Afshordi, N. Oshita, and Q. Wang, *Universe* **6**, 43 (2020), arXiv:2001.09553.
[21] E. Maggio, L. Buoninfante, A. Mazumdar, and P. Pani, *Phys. Rev. D* **102**, 064053 (2020), arXiv:2006.14628.
[22] J.B. Hartle, *Phys. Rev.* **D8**, 1010 (1973).
[23] S.A. Hughes, *Phys. Rev. D* **64**, 064004 (2001).
[24] E. Poisson and C. Will, *Gravity: Newtonian, Post-Newtonian, Relativistic* (Cambridge University Press, Cambridge, UK, 1953).
[25] K. Alvi, *Phys. Rev.* **D64**, 104020 (2001), arXiv:gr-qc/0107080.
[26] A. Maselli, P. Pani, V. Cardoso, T. Abdelsalhin, L. Gualtieri, and V. Ferrari, *Phys. Rev. Lett.* **120**, 081101 (2018), arXiv:1703.10612.
[27] S.A. Hughes, *Phys. Rev. D* **64**, 064004 (2001), [Erratum: Phys.Rev.D 88, 109902 (2013)], arXiv:gr-qc/0104041.
[28] S. Bernuzzi, A. Nagar, and A. Zenginoglu, *Phys. Rev. D* **86**, 104038 (2012), arXiv:1207.0769.
[29] A. Taracchini, A. Buonanno, S.A. Hughes, and G. Khanna, *Phys. Rev. D* **88**, 044001 (2013), [Erratum: Phys.Rev.D 88, 109903 (2013)], arXiv:1305.2184.
[30] E. Harms, S. Bernuzzi, A. Nagar, and A. Zenginoglu, *Class. Quant. Grav.* **31**, 245004 (2014), arXiv:1406.5983.
[31] S. Datta, R. Brito, S. Bose, P. Pani, and S.A. Hughes, *Phys. Rev. D* **101**, 044004 (2020), arXiv:1910.07841.
[32] H. Audley *et al.*, (2017), arXiv:1702.00786.
[33] S. Datta, *Phys. Rev. D* **102**, 064040 (2020), arXiv:2002.04480.
[34] F.D. Ryan, *Phys. Rev. D* **52**, 5707 (1995).
[35] L. Barack and C. Cutler, *Phys. Rev. D* **75**, 042003 (2007), arXiv:gr-qc/0612029.
[36] S. Babak, J. Gair, A. Sesana, E. Barausse, C.F. Sopuerta, C.P.L. Berry, E. Berti, P. Amaro-Seoane, A. Petiteau, and A. Klein, *Phys. Rev. D* **95**, 103012 (2017), arXiv:1703.09722.
[37] M. Bianchi, D. Consoli, A. Grillo, J.F. Morales, P. Pani, and G. Raposo, *Phys. Rev. Lett.* **125**, 221601 (2020), arXiv:2007.01743.
[38] I. Bah, I. Bena, P. Heidmann, Y. Li, and D.R. Mayerson, (2021), arXiv:2104.10686.
[39] C.F. Sopuerta and N. Yunes, *Phys. Rev. D* **80**, 064006 (2009), arXiv:0904.4501.
[40] N. Yunes, P. Pani, and V. Cardoso, *Phys. Rev. D* **85**, 102003 (2012), arXiv:1112.3351.
[41] P. Pani, V. Cardoso, and L. Gualtieri, *Phys. Rev. D* **83**, 104048 (2011), arXiv:1104.1183.
[42] V. Cardoso, G. Castro, and A. Maselli, *Phys. Rev. Lett.* **121**, 251103 (2018), arXiv:1809.00673.
[43] A. Maselli, N. Franchini, L. Gualtieri, and T.P. Sotiriou, *Phys. Rev. Lett.* **125**, 141101 (2020), arXiv:2004.11895.
[44] P. Pani and A. Maselli, *Int. J. Mod. Phys. D* **28**, 1944001 (2019), arXiv:1905.03947.
[45] J.R. Gair, M. Vallisneri, S.L. Larson, and J.G. Baker, *Living Rev.Rel.* **16**, 7 (2013), arXiv:1212.5575.
[46] V. Baibhav *et al.*, (2019), arXiv:1908.11390.
[47] E. Barausse *et al.*, *Gen. Rel. Grav.* **52**, 81 (2020), arXiv:2001.09793.
[48] P. Pani, E. Berti, V. Cardoso, Y. Chen, and R. Norte, *Phys. Rev.* **D80**, 124047 (2009), arXiv:0909.0287.
[49] P. Pani, E. Berti, V. Cardoso, Y. Chen, and R. Norte, *Phys. Rev.* **D81**, 084011 (2010), arXiv:1001.3031.
[50] C.F.B. Macedo, P. Pani, V. Cardoso, and L.C.B. Crispino, *Phys. Rev.* **D88**, 064046 (2013), arXiv:1307.4812.
[51] V. Cardoso, A. del Rio, and M. Kimura, *Phys. Rev. D* **100**, 084046 (2019), [Erratum: Phys.Rev.D 101, 069902 (2020)], arXiv:1907.01561.
[52] K. Fransen, G. Koekoek, R. Tielemans, and B. Vercnocke, (2020), arXiv:2005.12286.
[53] N. Oshita, Q. Wang, and N. Afshordi, *JCAP* **04**, 016 (2020), arXiv:1905.00464.
[54] E. Barausse, R. Brito, V. Cardoso, I. Dvorkin, and P. Pani, *Class. Quant. Grav.* **35**, 20LT01 (2018), arXiv:1805.08229.
[55] G. Raposo, P. Pani, and R. Emparan, (2018), arXiv:1812.07615.
[56] P. Pani, *Phys. Rev.* **D92**, 124030 (2015), arXiv:1506.06050.
[57] N. Uchikata and S. Yoshida, *Class. Quant. Grav.* **33**, 025005 (2016), arXiv:1506.06485.
[58] N. Uchikata, S. Yoshida, and P. Pani, *Phys. Rev.* **D94**, 064015 (2016), arXiv:1607.03593.
[59] K. Yagi and N. Yunes, *Phys. Rev.* **D91**, 123008 (2015), arXiv:1503.02726.
[60] K. Yagi and N. Yunes, *Phys. Rev.* **D91**, 103003 (2015), arXiv:1502.04131.
[61] C. Posada, *Mon. Not. Roy. Astron. Soc.* **468**, 2128 (2017), arXiv:1612.05290.
[62] B. Guo, S. Hampton, and S.D. Mathur, *JHEP* **07**, 162 (2018), arXiv:1711.01617.
[63] S. Xin, B. Chen, R.K.L. Lo, L. Sun, W.B. Han, X. Zhong, M. Srivastava, S. Ma, Q. Wang, and Y. Chen, (2021), arXiv:2105.12313.
[64] N. Sago and T. Tanaka, *PTEP* **2020**, 123E01 (2020), arXiv:2009.08086.
[65] S.A. Teukolsky, *Phys. Rev. Lett.* **29**, 1114 (1972).
[66] S.A. Teukolsky, *Astrophys. J.* **185**, 635 (1973).
[67] S.A. Teukolsky and W.H. Press, *Astrophys. J.* **193**, 443 (1974).

[68] R. Fujita and H. Tagoshi, *Prog. Theor. Phys.* **112**, 415 (2004), arXiv:gr-qc/0410018.

[69] S.A. Hughes, *Phys. Rev. D* **61**, 084004 (2000), [Erratum: Phys.Rev.D 63, 049902 (2001), Erratum: Phys.Rev.D 65, 069902 (2002), Erratum: Phys.Rev.D 67, 089901 (2003), Erratum: Phys.Rev.D 78, 109902 (2008), Erratum: Phys.Rev.D 90, 109904 (2014)], arXiv:gr-qc/9910091.

[70] S. Detweiler, *Proceedings of the Royal Society of London Series A* **352**, 381 (1977).

[71] T. Hinderer and E.E. Flanagan, *Phys. Rev.* **D78**, 064028 (2008), arXiv:0805.3337.

[72] G.A. Piovano, A. Maselli, and P. Pani, *Phys. Rev. D* **102**, 024041 (2020), arXiv:2004.02654.

[73] V. Cardoso, L.C.B. Crispino, C.F.B. Macedo, H. Okawa, and P. Pani, *Phys. Rev.* **D90**, 044069 (2014), arXiv:1406.5510.

[74] J.L. Friedman, *Communications in Mathematical Physics* **63**, 243 (1978).

[75] S. Yoshida and Y. Eriguchi, *Monthly Notices of the Royal Astronomical Society* **282**, 580 (1996), https://academic.oup.com/mnras/article-pdf/282/2/580/3511331/282-2-580.pdf.

[76] V. Cardoso, P. Pani, M. Cadoni, and M. Cavaglia, *Phys. Rev.* **D77**, 124044 (2008), arXiv:0709.0532.

[77] V. Cardoso, P. Pani, M. Cadoni, and M. Cavaglia, *Class. Quant. Grav.* **25**, 195010 (2008), arXiv:0808.1615.

[78] P. Pani, E. Barausse, E. Berti, and V. Cardoso, *Phys. Rev.* **D82**, 044009 (2010), arXiv:1006.1863.

[79] T. Robson, N.J. Cornish, and C. Liu, *Class. Quant. Grav.* **36**, 105011 (2019), arXiv:1803.01944.

[80] B. Allen, W.G. Anderson, P.R. Brady, D.A. Brown, and J.D.E. Creighton, *Phys. Rev. D* **85**, 122006 (2012), arXiv:gr-qc/0509116.

[81] M. van de Meent, *Phys. Rev. D* **90**, 044027 (2014), arXiv:1406.2594.

[82] M. van de Meent and A.G. Shah, *Phys. Rev. D* **92**, 064025 (2015), arXiv:1506.04755.

[83] M. van de Meent, *Phys. Rev. D* **94**, 044034 (2016), arXiv:1606.06297.

[84] M. van de Meent, *Phys. Rev. D* **97**, 104033 (2018), arXiv:1711.09607.

[85] S. Mano, H. Suzuki, and E. Takasugi, **95**, 1079 (1996), arXiv:gr-qc/9603020.

[86] S. Mano and E. Takasugi, **97**, 213 (1997), arXiv:gr-qc/9611014.

[87] R. Fujita, W. Hikida, and H. Tagoshi, *Prog. Theor. Phys.* **121**, 843 (2009), arXiv:0904.3810.

[88] A. Ori and K.S. Thorne, *Phys. Rev. D* **62**, 124022 (2000), arXiv:gr-qc/0003032.

[89] J.A. Pons, E. Berti, L. Gualtieri, G. Miniutti, and V. Ferrari, *Phys. Rev.* **D65**, 104021 (2002), arXiv:gr-qc/0111104.

[90] S.J. Kapadia, D. Kennefick, and K. Glampedakis, *Phys. Rev. D* **87**, 044050 (2013), arXiv:1302.1016.

[91] V. Cardoso, S. Chakrabarti, P. Pani, E. Berti, and L. Gualtieri, *Phys. Rev. Lett.* **107**, 241101 (2011), arXiv:1109.6021.

[92] L. Lindblom, B.J. Owen, and D.A. Brown, *Phys. Rev.* **D78**, 124020 (2008), arXiv:0809.3844.

[93] B. Bonga, H. Yang, and S.A. Hughes, *Phys. Rev. Lett.* **123**, 101103 (2019), arXiv:1905.00030.

[94] E.E. Flanagan and S.A. Hughes, *Phys. Rev.* **D57**, 4566 (1998), arXiv:gr-qc/9710129.

[95] Q. Wang, N. Oshita, and N. Afshordi, *Phys. Rev. D* **101**, 024031 (2020), arXiv:1905.00446.

[96] B. Chen, Q. Wang, and Y. Chen, *Phys. Rev. D* **103**, 104054 (2021), arXiv:2012.10842.

[97] L. Barack, *Class. Quant. Grav.* **26**, 213001 (2009), arXiv:0908.1664.

[98] E. Poisson, A. Pound, and I. Vega, *Living Rev. Rel.* **14**, 7 (2011), arXiv:1102.0529.

[99] A. Pound and B. Wardell, (2021), arXiv:2101.04592.

[100] A.J.K. Chua, N. Korsakova, C.J. Moore, J.R. Gair, and S. Babak, *Phys. Rev. D* **101**, 044027 (2020), arXiv:1912.11543.

[101] M.L. Katz, A.J.K. Chua, L. Speri, N. Warburton, and S.A. Hughes, (2021), arXiv:2104.04582.

[102] G.A. Piovano, R. Brito, A. Maselli, and P. Pani, (2021), arXiv:2105.07083.